the appearance of endpoints on glass transitions lines where the difference between two glasses vanishes (*19*). Close to such points, the structural relaxation will exhibit an especially broad distribution of relaxation times, because the system anticipates arrest in either of two glassy structures. Sample C (inset, Fig. 3) displays rather anomalous, stretched-out dynamics over an appreciable range in time. The functional form of this dynamics is consistent with MCT predictions (*25*) as well as simulations (*26*).

A model hard-sphere colloid with a short-range attraction induced by added polymer shows a reentrant glass transition at high densities. This system is sufficiently well characterized that we were able to compare our observations with MCT calculations with no adjustable parameters. These calculations, molecular dynamics simulations, and light-scattering experiments all suggest that the reentrance is due to the existence of two qualitatively distinct kinds of glasses, dominated by repulsion and attraction, respectively (*27*). Sticky hard spheres are also predicted to show an isostructural crystal-crystal transition (*28*). If the stickiness is modeled by a square well, this transition vanishes when the well width is between 6 and 7% of the hard core (*28*), whereas the glass-glass transition disappears at ~5% attraction width (*19*). The similarity is striking: The same mechanism, a competition between attraction and repulsion, underlies both phenomena.

References and Notes

1. See the wide-ranging survey articles in *Science* **267**, 1887 (1995) and particularly (*2*, *3*).
2. C. A. Angell, *Science* **267**, 1924 (1995).
3. F. H. Stillinger, *Science* **267**, 1935 (1995).
4. J. D. Bernal, *Proc. R. Soc. London Ser. A* **280**, 299 (1964).
5. U. Bengtzelius, W. Götze, A. Sjölander, *J. Phys. C* **17**, 5915 (1984)
6. P. N. Pusey, W. van Megen, *Nature* **320**, 340 (1986).
7. ———, *Phys. Rev. Lett.* **59**, 2083 (1987).
8. See the review and references cited in W. Götze, *J. Phys. Condens. Matter* **11**, A1 (1999).
9. E. R. Weeks, J. C. Crocker, A. C. Levitt, A. Schofield, D. A. Weitz, *Science* **287**, 627 (2000).
10. W. G. Hoover, F. H. Ree, *J. Chem. Phys.* **49**, 3609 (1968).
11. D. Rudhardt, C. Bechinger, P. Leiderer, *Phys. Rev. Lett.* **81**, 1330 (1998).
12. S. Asakura, F. Oosawa, *J. Chem. Phys.* **22**, 1255 (1954).
13. W. C. K. Poon, A. D. Pirie, P. N. Pusey, *Faraday Discuss.* **101**, 65 (1995).
14. W. C. K. Poon *et al.*, *Faraday Discuss.* **112**, 143 (1999).
15. H. N. W. Lekkerkerker *et al.*, *Europhys. Lett.* **20**, 559 (1992).
16. Even at the highest polymer concentrations reached in this work, we are still considerably below the overlap concentration $c^* \sim 30$ mg cm^{-3}, where the effective coil volume fraction is ~1.
17. We calculated $S(q)$ for hard spheres with an attractive Yukawa tail in the mean spherical approximation and exploited a mapping to the AO attraction tail. State points are paired up for $\phi \rightarrow 0$ by equating the large-q behavior of the Mayer functions (amplitude A and period ξ' of oscillation) in the limits $\xi \rightarrow 0$ and for strong attractions. A is connected to the polymer concentration and ξ' to the polymer size. The adequacy of this mapping has been confirmed by Monte Carlo simulations at a number of AO state points. The dominant uncertainty when comparing the theory and simulations to the experiments arises from the unknown many-body effects not captured in the AO potential. We expect that AO overestimates the effective strength of the attraction. MCT predicts $\phi_g = 0.52$ for hard spheres (HS); we apply a scaling factor 0.58/0.52 to agree with the experimental value of $\phi_g^{HS} = 0.58$.
18. The MCT ideal-glass criterion is when $S(q,t \rightarrow \infty) > 0$. In Fig. 1 we show where crystallization was not observed on the week/month time scale, which is at least indicative of a nearby glass transition.
19. K. Dawson *et al.*, *Phys. Rev. E* **63**, 011401 (2000) and references therein.
20. A flat top-hat distribution of particle size with polydispersity 10% was chosen, and a smooth repulsive potential barrier of maximal height 1 k_BT (the thermal energy) and width $2R(1 - \xi)$ modeled by a quartic polynomial which gives continuous total force was added. For computational efficiency and because we are interested in the long-time structural relaxation only, Newtonian (rather than Brownian) dynamics was used.
21. P. N. Segrè *et al.*, *J. Mod. Opt.* **42**, 1929 (1995).
22. W. van Megen, S. M. Underwood, *Phys. Rev. E* **49**, 4206 (1994).
23. Direct comparison with (*22*) is complicated by differing polydispersities, which lead to differing random-close-packing densities, ϕ_{rcp}: The particle dynamics is a very sensitive function of $f = (\phi_{rcp} - \phi)/\phi_{rcp}$ near ϕ_{rcp}. We measured $\phi_{rcp} \sim 0.68$ for our particles. Our data for sample *A*, which has $f = 0.1$, are consistent with what van Megen and Underwood showed at comparable wavevectors for a sample with $\phi = 0.578$ (see their figure 6a). They took $\phi_{rcp} = 0.64$, so that $\phi = 0.578$ corresponds to $f = 0.097$.
24. The $f(q,t)$ data (Fig. 3) indicate the freezing-in of large collective density fluctuations, whereas the $\langle r^2(t) \rangle$ data (Fig. 2) suggest strongly localized single-particle motion.
25. The scattering function for sample C is compatible with logarithmic decay, $S(q,t) = F(q) - H(q)\log(t/t_*)$, over more than a decade in time, as predicted by MCT for state points close to where the glass-glass transition should vanish (*19*). Such dynamics have been observed before in less well-characterized systems (*29*, *30*).
26. A. M. Puertas, M. Fuchs, M. E. Cates, *Phys. Rev. Lett.* **88**, 098301 (2002).
27. The existence of multiple glassy states in a single material has been suggested in atomic systems [such as SiO_2 and GeO_2 (*31*) and water (*32*)]. The underlying physics in these network formers (*33*), however, is almost certainly distinct from that we have reported here for the simple model system of sticky hard spheres.
28. P. Bolhuis, M. Hagen, D. Frenkel, *Phys. Rev. E* **50**, 4880 (1994).
29. F. Mallamace *et al.*, *Phys. Rev. Lett.* **84**, 5431 (2000).
30. E. Bartsch, M. Antonietti, W. Schupp, H. Sillescu, *J. Chem. Phys.* **97**, 3950 (1992).
31. O. B. Tsiok *et al.*, *Phys. Rev. Lett.* **80**, 999 (1998).
32. O. Mishima, Y. Suzuki, *J. Chem. Phys.* **115**, 4199 (2001).
33. G. Franzese *et al.*, *Nature* **409**, 692 (2001).

34. K.N.P. holds a UK Overseas Research Studentship and is partially supported by the University of Edinburgh. A.M.P., J.B., and M.F. were funded by the Ministerio de Educación y Cultura, Spain; the Swedish National Science Research Council; and the Deutsche Forschungsgemeinschaft (grant Fu 309/3), respectively.

20 November 2001; accepted 22 February 2002

Layer-by-Layer Growth of Binary Colloidal Crystals

Krassimir P. Velikov,* Christina G. Christova,[1] Roel P. A. Dullens,[1]† Alfons van Blaaderen[1,2]*

We report the growth of binary colloidal crystals with control over the crystal orientation through a simple layer-by-layer process. Well-ordered single binary colloidal crystals with a stoichiometry of large (L) and small (S) particles of LS_2 and LS were generated. In addition, we observed the formation of an LS_3 superstructure. The structures formed as a result of the templating effect of the first layer and the forces exerted by the surface tension of the drying liquid. By using spheres of different composition, one component can be selectively removed, as is demonstrated in the growth of a hexagonal non–close-packed colloidal crystal.

A mixture of submicrometer or colloidal particles of two sizes can self-organize into two-dimensional (2D) (*1*) and 3D (*2*–*6*) binary crystals, which can have different stoichiometries and crystal symmetries depending on the size ratio and concentration. Binary colloidal crystals of large (L) and small (S) particles were first observed in nature. Two types of structures, with stoichiometry LS_2 (atomic analog AlB_2) and LS_{13} (atomic analog $NaZn_{13}$), were found in Brazilian opals (*3*). Later, binary crystals were observed in suspensions of charge-stabilized polystyrene (*4*) and of hard sphere–like PMMA (*5*) particles. Formation of small 2D binary crystals was observed in a mixture of alkanethiol-derivatized Au nanoparticles although it is unclear whether the formation of these crystals was determined by thermodynamics alone (*1*). However, binary crystals have not

[1]Soft Condensed Matter, Debye Institute, Utrecht University, Princetonlaan 5, 3584 CC Utrecht, Netherlands. [2]FOM Institute for Atomic and Molecular Physics, Kruislaan 407, 1098 SJ Amsterdam, Netherlands.

*To whom correspondence should be addressed. E-mail: k.p.velikov@phys.uu.nl, a.vanblaaderen@phys.uu.nl

†Present address: Van't Hoff Laboratory for Physical and Colloid Chemistry, Debye Institute, Utrecht University, Padualaan 8, 3584 CH Utrecht, Netherlands.

been investigated as extensively as one-component colloidal crystals mainly because they are harder to grow and characterize.

It has been shown that entropy alone is sufficient to cause bulk crystallization of LS_2 and LS_{13} crystals from a mixture of hard spheres of two sizes (*6*). At volume fractions that are substantially higher than the equilibrium volume fractions, packing arguments can be used to predict which crystal phase will form (*2*, *3*). Colloidal epitaxy (*7*, *8*) and a form of controlled drying on a substrate (*9*–*11*) have been developed to control the size and orientation of crystals of a single colloidal material grown in bulk. In the controlled drying technique, a colloidal crystal is formed at the drying front of an evaporating dispersion with a relatively low volume fraction of particles. Particles are transported to and concentrated at the drying edge by a fluid flow induced by the evaporation. The crystallization is driven not only by a lowering of the free energy but also by the influence of surface-tension effects exerted on particles that are protruding through the drying meniscus (*11*) and by the templating action of particles that are already deposited (*7*). With this nonequilibrium process, it is possible to grow large (~mm^2) single 2D (*12*) and 3D (*10*) colloidal crystals with precise control over the thickness through the particle volume fraction (*10*, *13*).

We report the fabrication of binary colloidal crystals using a controlled drying process on a vertical substrate in a layer-by-layer fashion. A 2D hexagonal close-packed crystal of large (L) silica spheres (R_L = 203 nm) (*14*) was grown on a clean glass substrate with a growth rate of 1 to 2 mm per day. The 2D crystal was used as a template on which small (S) silica or polystyrene particles were deposited. The small particles (R_S = 101- or 110-nm silica, or 97-nm polystyrene) arranged themselves in regular structures depending on their volume fraction, ϕ, and on the size ratio, $\gamma = R_S/R_L$. Another layer of large particles was then deposited, and these steps were successively repeated to grow a 3D structure of the desired thickness and composition. We studied a narrow range of size ratios, γ = 0.48 to 0.54, where we expected LS_2 on the basis of experimental observations in bulk crystallization (*4*, *5*) and on the basis of packing arguments (*3*).

For γ = 0.54 and a relatively high $\phi = 4.3 \times 10^{-4}$, a slightly corrugated but "complete" close-packed layer of small particles on top of the large ones was observed (*15*). Decrease of the volume fraction to $\phi = 2.1 \times 10^{-4}$ led to the formation of large (~200 μm^2) areas with a hexagonal, but more open, packing (*16*) with three neighbors (Fig. 1A). Here the small spheres filled in all the hexagonally arranged crevices made by the first layer of larger spheres. The next layer of large particles deposited itself exactly on top of the first layer, as expected (Fig. 1, B and C), which leads to the formation of the well-known LS_2 binary colloidal crystal (Fig. 1D). The preserved order of the small spheres can be seen through a patch in the crystal that had an incomplete top layer (Fig. 1B). Continued layer-by-layer deposition leads to an LS_2 binary colloidal crystal of desired thickness with exactly the same AlB_2 structure (Fig. 1D) that is observed in bulk colloidal crystallization (*5*). We have grown four layers of LS_2 crystals that are large enough (several hundred micrometers) to be investigated by optical transmission measurements. Stacking faults in this structure during the layer-by-layer growth are not possible because the optimal positions of small and large particles are uniquely defined in each growth step. The incomplete layers of large spheres shown in Fig. 1B (and below in Figs. 2B and 3B) are shown only to evaluate the orientation of the layer of small particles below. Large "complete" layers several hundred micrometers thick, like those shown in Fig. 1C, were grown, but are not very illustrative in a scanning electron micrograph (SEM).

A further decrease in the volume fraction led to the formation of another open structure with hexagonal symmetry. This structure, with stoichiometry LS, is similar to LS_2, but instead of six particles, there are now three small particles touching each large one. Figure 2A shows a large region formed by polystyrene particles ($\phi = 1.1 \times 10^{-4}$, γ = 0.48) on a 2D crystal of large silica particles. The small particles unexpectedly retain a long-range hexagonal order (see the Fourier transform in Fig. 2C), even when they are not touching. The next layer of larger particles can now stack in one of two positions: exactly on top of the first layer as for the LS_2 structure (AA stacking) or into the crevices that are not occupied by the small particles formed by the first hexagonal layer (AB

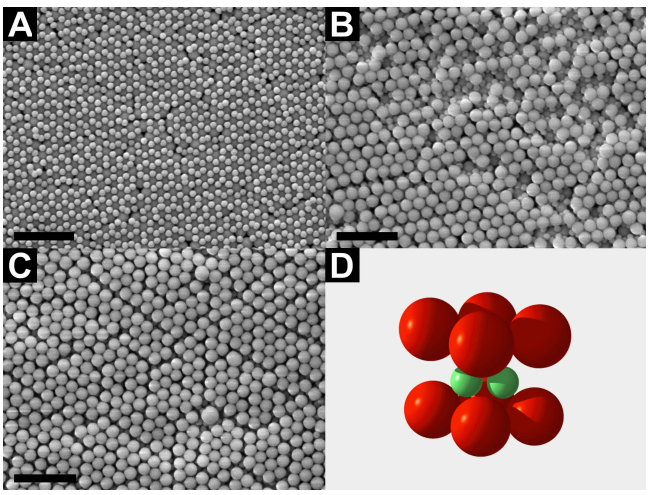

Fig. 1. SEM showing binary colloidal crystals (size ratio, γ = 0.54) with a stoichiometry LS_2. (**A**) Open packing with hexagonal symmetry where each small sphere has three neighbors on top of a 2D crystal of large spheres. (**B**) An incomplete third layer of large particles that shows the structure of the layer underneath. (**C**) Well-ordered complete third layer of large spheres. (**D**) Schematic presentation of the unit cell of an LS_2 binary crystal. Bars, 2 μm.

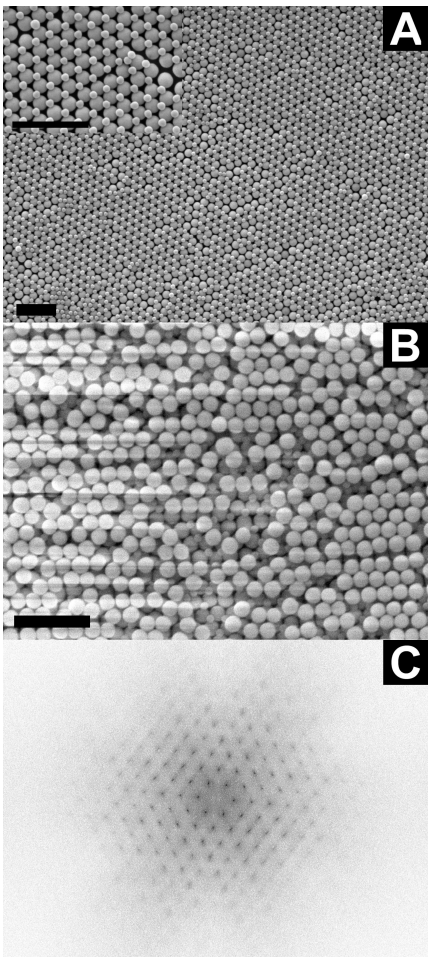

Fig. 2. SEM showing binary colloidal crystals (γ = 0.48) with a stoichiometry LS. (**A**) Small spheres ordered in an open hexagonal lattice on top of a 2D crystal of large spheres. (**B**) An incomplete third layer of large particles shows that the large spheres deposit in the interstices not occupied by the small spheres. (**C**) Fourier transform of (A) after assigning the large and small particles similar gray values. Bars, 2 μm.

stacking). For $\gamma = 0.48$, the next layer always grows as an AB sequence of the larger spheres. This configuration has a higher packing density (Fig. 2B), although it is possible that this preference for AB stacking of the large spheres is lost for large values of γ. For the fourth layer, formed from small particles, we did not expect any preferred orientation with respect to the second layer of small particles. This was indeed confirmed by observation and leads to ambiguity in the stacking of the resulting 3D structure. Therefore, only randomly stacked analogs of NaCl or NiAs can be grown by our layer-by-layer method. Although binary colloidal crystals of NaCl type have been predicted to be a stable phase in bulk crystallization (*17*), small crystallites of binary crystal of stoichiometry LS were only recently observed (*18*). It was not clear whether this structure was a pure NaCl crystal or whether it was a random-stacked crystal.

For size ratios of $\gamma = 0.48$ to 0.5, a completely different arrangement of the small spheres, in addition to the LS and LS_2 structures described above, was observed. Again, at a relatively high volume fraction ($\phi = 4.1 \times 10^{-4}$, $\gamma = 0.48$) of the small particles, a "complete" coverage on the top of the large particles was seen [Web fig. 1 (*19*)]. At lower volume fractions ($\phi = 2.1 \times 10^{-4}$), an arrangement of the small spheres on top of the 2D crystal of large spheres was observed; in this case, each small sphere had four neighbors (*16*) (Fig. 3A). Similar to the LS_2 binary crystal, each large sphere was surrounded in a ring by six small spheres, but the rings were rotated in such a way that the crevices that formed in-between the large spheres were filled with three small spheres arranged in a (planar) triangle (Fig. 3A). In general, this open structure was found to coexist with the LS_2 structure [Web fig. 2 (*19*)] observed previously or with a complete layer of small particles [Web fig. 1 (*19*)]. A structure with this symmetry is known in the field of antiferromagnetics as a kagomé lattice. In this field, an arrangement of spins with this symmetry is a well-known example of a geometrically frustrated lattice, which cannot order because of the high degeneracy of its ground state and ensuing large fluctuations (*20*). Deposition of a second layer of large particles led to the formation of an LS_3 binary colloidal crystal (Fig. 3B). As with the LS_2 crystal, degeneracy in stacking is not possible because the position of each successive layer is unambiguously defined. To our knowledge, LS_3 does not have a reported isostructural binary atomic analog. It has a higher packing fraction than LS_2 for $\gamma < 0.48$ [Web fig. 3 (*19*)] and should therefore be the thermodynamically stable phase at high pressure. However, as far as we are aware, it has not been studied theoretically or ever suggested before as a possible binary colloidal crystal.

The complex self-organization of the small particles in the second layer is the result of the interplay of geometrical packing arguments, minimization of the surface free energy of the drying liquid film, and surface forces due to the curved menisci. During the drying process, particles partially immersed experience attractive capillary forces (*12*) and the corrugated surface of the first layer of large particles. Because the drying rate is constant, the specific packing that is obtained is determined by the local particle concentration and the symmetry and orientation of the already deposited layers. A schematic representation of the process is shown in Fig. 4. We inferred this mechanism by studying the defects that formed [Web fig. 4 (*19*)] and by our observation that a crystal of spheres of one size that is deposited in a controlled drying procedure is oriented in such a way that the lines of particles forming the hexagonal (111) planes are parallel to the drying front. Such an arrangement of particles at the interface of the drying liquid can explain this observation. At sufficiently high volume fraction the second layer of smaller particles also forms a 2D hexagonal layer with lines of touching particles parallel to the drying front (Fig. 4). Even though this layer cannot be flat—e.g., the darker particles in the figure are elevated because they are exactly on top of the particles in the first layer—the size ratio of ~0.5 makes it geometrically possible for the second layer to become hexagonal as well. At slightly lower volume fraction, ϕ_3, complete coverage by the second layer is not possible, so that the dark particles (Fig. 4), which protrude from the drying film the most, are lost first. This leads to the kagomé net observed for the second layer in Fig. 3. At an even lower lower volume fraction, ϕ_2, the structures formed can again explained by taking fewer particles in the drying front and placing them at the lowest points that become available. These are formed by the hexagonal crevices formed by the hexagonally arranged first layer. This structure has the LS_2 arrange-

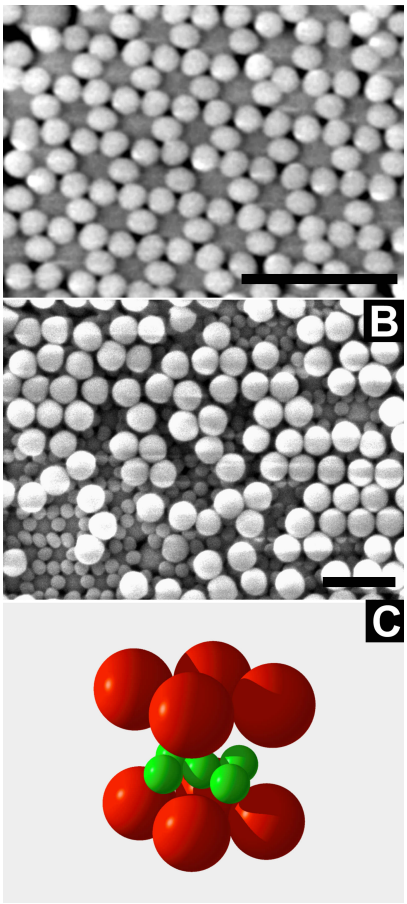

Fig. 3. SEM showing binary colloidal crystals ($\gamma = 0.50$) with stoichiometry LS_3. (**A**) A magnified region with a kagomé net of small spheres on top of a 2D crystal of large spheres. (**B**) An incomplete third layer of large particles. (**C**) Schematic presentation of the unit cell of an LS_3 binary crystal. Bars, 1 μm.

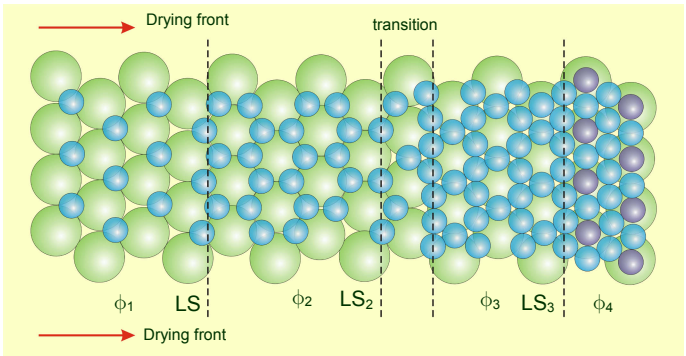

Fig. 4. Schematic representation of the structures of small spheres, with size ratio of ~0.5, that form onto a 2D hexagonal layer of larger spheres, as a function of the volume fraction. The symmetry of the structures can be understood as resulting from the templating effect of the first layer and the forces resulting from the particle-liquid interfacial tension. Particles are lined parallel to the drying front and project into those places that lie lowest on the 2D crystalline layer of the larger particles. The volume fraction, ϕ, determines how many of the available low-lying sites will ultimately be occupied. See also the defect structures and structures at ϕ_4 in Web figs. 1 and 4 (*19*).

ment shown in Fig. 1. Because the change in volume fraction from ϕ_3 to ϕ_2 is quite subtle, the LS_3 structures are seen primarily in combination with the LS_2 and with defects in the transition region indicated in Fig. 4 [see Web figs. 1, 3, and 4 (*19*)]. At ϕ_1 there are even fewer particles in the drying front, and filling the lowest points in a line parallel to the drying film results in the LS structure from Fig. 2. Our observations also explain the finding (*21*) that in holes in a polymer film in which three particles fitted, the drying front arranged the triangles with sides parallel to the drying front.

To create non–close-packed crystals of single-sized particles with our method, we first created a composite LS_2 binary crystal of alternating layers of inorganic (silica) and organic (polystyrene) particles. Then, the organic layer was removed by heating (rate 1°C/min) in an oven at 600°C for 4 hours in air. The resulting structure is a hexagonal non–close-packed (hncp) crystal (Fig. 5). This non–close-packed structure, with a low packing fraction of $\rho = 0.6046$ compared with the close-packed structure ($\rho = 0.7405$), is another example of how the layer-by-layer method can be used to create new crystal structures that cannot be grown in bulk.

We have demonstrated the formation of large areas of LS, LS_2, and LS_3 binary colloidal crystals using a nonequilibrium layer-by-layer growth process. We have explored only a small region of γ values, and so there is a large scope for expanding on this work. The method is simple enough that it can be easily automated to create structures thicker than those shown here (*22*). By using surface templates (*7*), the method can be further extended by growing different crystal planes and new types of crystals with a well-defined crystal orientation (*23*). For example, using a square template will make it possible to grow CsCl-type binary structures. Our method may substantially expand the stoichiometries, compositions, and symmetries achievable with crystals of colloidal particles.

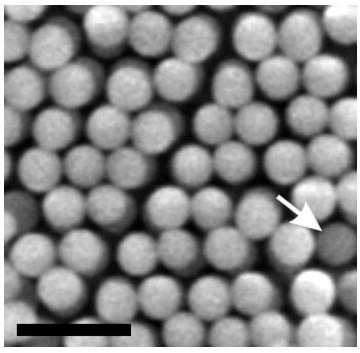

Fig. 5. SEM of the top layer of a hncp colloidal crystal. The arrow points to a particle from the bottom layer. Bar, 1 μm.

References and Notes

1. C. J. Kiely *et al.*, *Nature* **396**, 444 (1998).
2. M. J. Murray, J. V. Sanders, *Nature* **275**, 201 (1978).
3. _____, *Philos. Mag.* **43**, 721 (1980).
4. S. Hachisu, S. Yoshimura, *Nature* **283**, 188 (1980).
5. P. Bartlett, R. H. Ottewill, P. N. Pusey, *Phys. Rev. Lett.* **68**, 3801 (1992).
6. M. D. Eldridge, P. A. Madden, D. Frenkel, *Nature* **365**, 35 (1993).
7. A. van Blaaderen, R. Ruel, P. Wiltzius, *Nature* **385**, 321 (1997).
8. M. Heni, H. Lowen, *Phys. Rev. Lett.* **85**, 3668 (2000).
9. N. D. Denkov *et al.*, *Nature* **361**, 26 (1993).
10. P. Jiang, J. F. Bertone, K. S. Hwang, V. L. Colvin, *Chem. Mater.* **11**, 2132 (1999).
11. P. A. Kralchevsky, N. D. Denkov, *Curr. Opin. Colloid Interface Sci.* **6**, 383 (2001).
12. N. D. Denkov *et al.*, *Langmuir* **8**, 3183 (1992).
13. A. S. Dimitrov, K. Nagayama, *Langmuir* **12**, 1303 (1996).
14. Highly monodispersed silica particles (polydispersity $< 3\%$) were prepared by microemulsion (*24*) followed by seeded growth.
15. K. P. Velikov, C. G. Christova, R. P. A. Dullens, A. van Blaaderen, data not shown.
16. J. V. Smith, *Geometrical and Structural Crystallography* (Wiley, New York, 1982).
17. A. R. Denton, N. W. Ashcroft, *Phys. Rev. A* **42**, 7312 (1990).
18. N. Hunt, R. Jardine, P. Bartlett, *Phys. Rev. E* **62**, 900 (2000).
19. Supplementary Web material is available on *Science* Online at www.sciencemag.org/cgi/content/full/296/5565/106/DC1.
20. R. Moessner, S. L. Sondhi, *Phys. Rev. B* **6322**, 224401 (2001).
21. Y. D. Yin, Y. N. Xia, *Adv. Mater.* **13**, 267 (2001).
22. Because the mechanism underlying the controlled drying technique is similar to that of industrial coating processes, in which good control over the thickness of the depositing layers and high automatization are achieved, we believe that scaling up of the process to an industrial scale is feasible.
23. A. van Blaaderen, P. Wiltzius, *Adv. Mater.* **9**, 833 (1997).
24. K. Osseoasare, F. J. Arriagada, *Colloid Surf.* **50**, 321 (1990).

25. We thank P. M. Chaikin, A. Moroz, A. Imhof, and M. Dogterom for helpful discussions. This work is part of the research program of the Stichting voor Fundamenteel Onderzoek der Materie (FOM), which is financially supported by the Nederlandse Organisatie voor Wetenschappelijk Onderzoek.

16 October 2001; accepted 5 March 2002

Structure of Haloform Intercalated C_{60} and Its Influence on Superconductive Properties

Robert E. Dinnebier,[1] Olle Gunnarsson,[1] Holger Brumm,[1] Erik Koch,[1] Peter W. Stephens,[2] Ashfia Huq,[2] Martin Jansen[1]*

$CHCl_3$ and $CHBr_3$ intercalated C_{60} have attracted particular interest after a superconductivity transition temperature (T_c) of up to 117 K was discovered. We have determined the structure using synchrotron x-ray powder-diffraction and found that the expansion of the lattice mainly takes place in one dimension (triclinic *b* axis), leaving planes of C_{60} molecules on an approximately hexagonal, slightly expanded lattice. We have performed tight-binding band structure calculations for the surface layer. In spite of the slight expansion of the layers, for the range of dopings where a large T_c has been observed, the density of states at the Fermi energy is smaller for $C_{60}{\cdot}2CHCl_3$ and $C_{60}{\cdot}2CHBr_3$ than for C_{60}. This suggests that the lattice expansion alone cannot explain the increase of T_c.

Using a field-effect transistor (FET), Schön *et al.* have demonstrated that chemical doping is not the only way to make the fullerenes metallic and superconducting. They showed that pristine C_{60} can be field-doped and becomes superconducting with transition temperatures T_c up to 11 K for electron doping (*1*) and 52 K for hole doping (*2*). For the chemically electron-doped fullerenes, T_c increases with the lattice constant and is generally explained by the corresponding increase in the density of states (DOS) (*3*–*5*). This trend was the motivation for investigating fullerene crystals intercalated with inert molecules that act as spacers to expand the lattice. And, indeed, it was found that T_c increased to values of about 80 K for $C_{60}{\cdot}2CHCl_3$ and 117 K for $C_{60}{\cdot}2CHBr_3$, apparently confirming the assumption that in order to increase T_c one simply has to increase the DOS (*6*).

We report structure determinations of the $C_{60}{\cdot}2CHCl_3$ and $C_{60}{\cdot}2CHBr_3$ cocrystals and give a comparison with pristine C_{60}, finding that intercalation of chloroform and bromoform does increase the volume per C_{60} molecule. However, the increase is anisotropic and is mainly due to an expansion of the lattice perpendicular to the close-packed

[1]Max-Planck-Institut für Festkörperforschung, Heisenbergstrasse 1, D-70569 Stuttgart, Germany. [2]Department of Physics and Astronomy, State University of New York, Stony Brook, NY 11974, USA.

*To whom correspondence should be addressed. E-mail: m.jansen@fkf.mpg.de

Supplementary Material

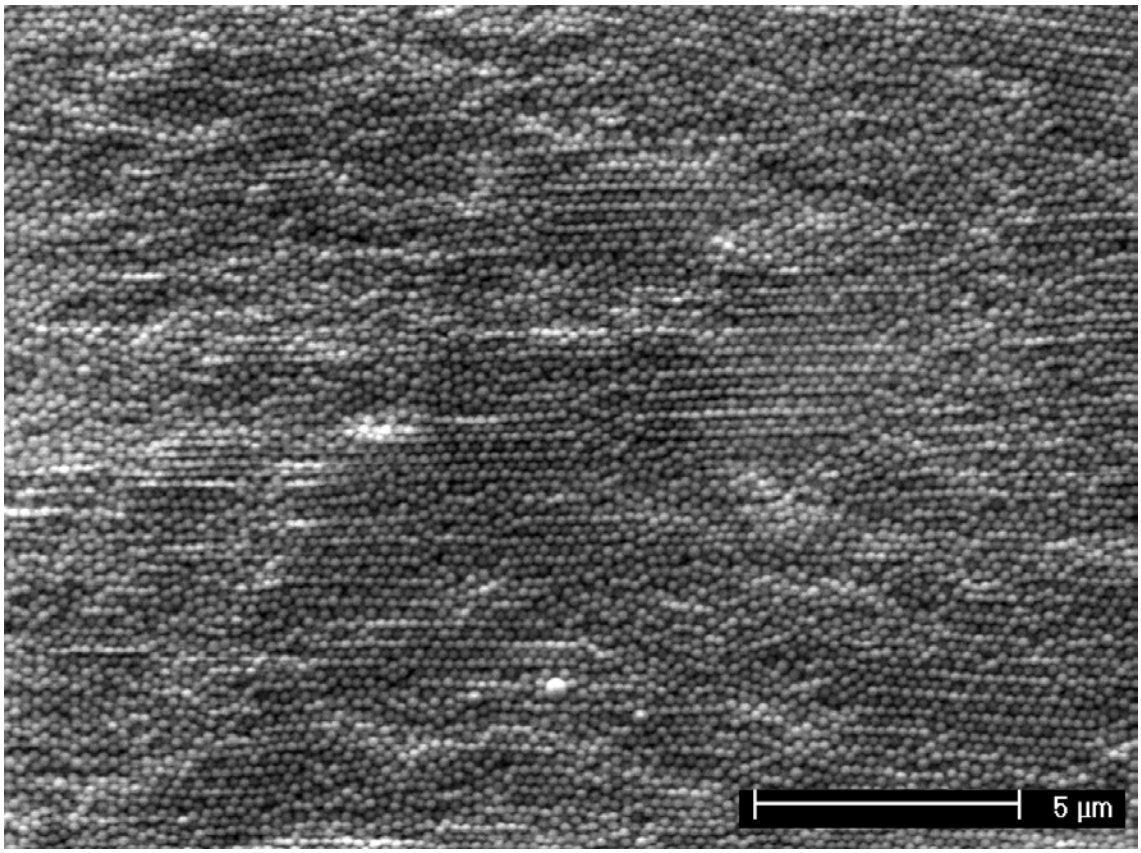

Supplemental Figure 1. Scanning electron micrographs (SEM) showing areas with *kagomé* symmetry of small spheres on top of a 2D crystal of large spheres ($\gamma = 0.48$), which co-exist with a 'complete' close-packed layer of small spheres.

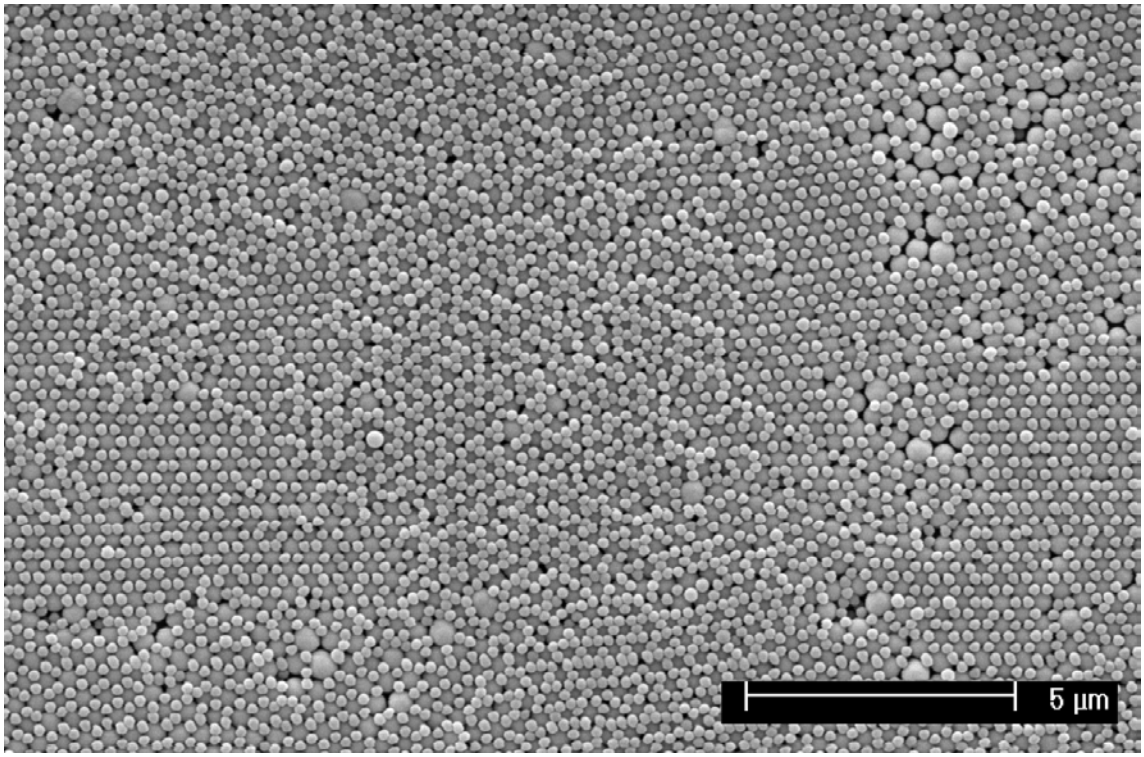

Supplemental Figure 2. Scanning electron micrographs (SEM) showing areas with *kagomé* symmetry of small spheres on top of a 2D crystal of large spheres (γ = 0.48) co-existin with an LS_2 net of small spheres.

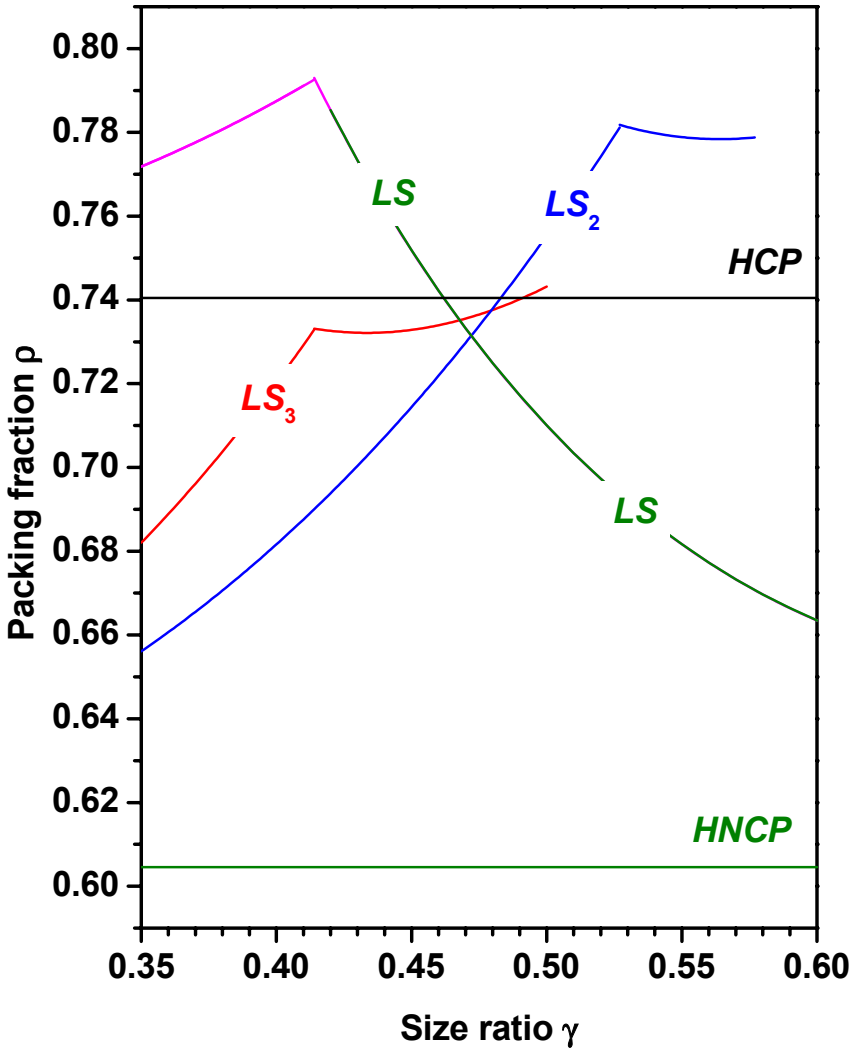

Supplemental Figure 3. Packing fraction diagram as a function of the size ratio γ for the *LS* (*NaCl* type), LS_2 (AlB_2 type), and LS_3 binary colloidal crystals. The calculations are performed only for touching large spheres in the basal plane. The packing limits of hexagonal close-packed (0.7405) and hexagonal non-close-packed (0.6046) crystals of one-size spheres are shown by horizontal lines. Note that the new LS_3 structure has a higher packing fraction than LS_2 for $\gamma < 0.48$.

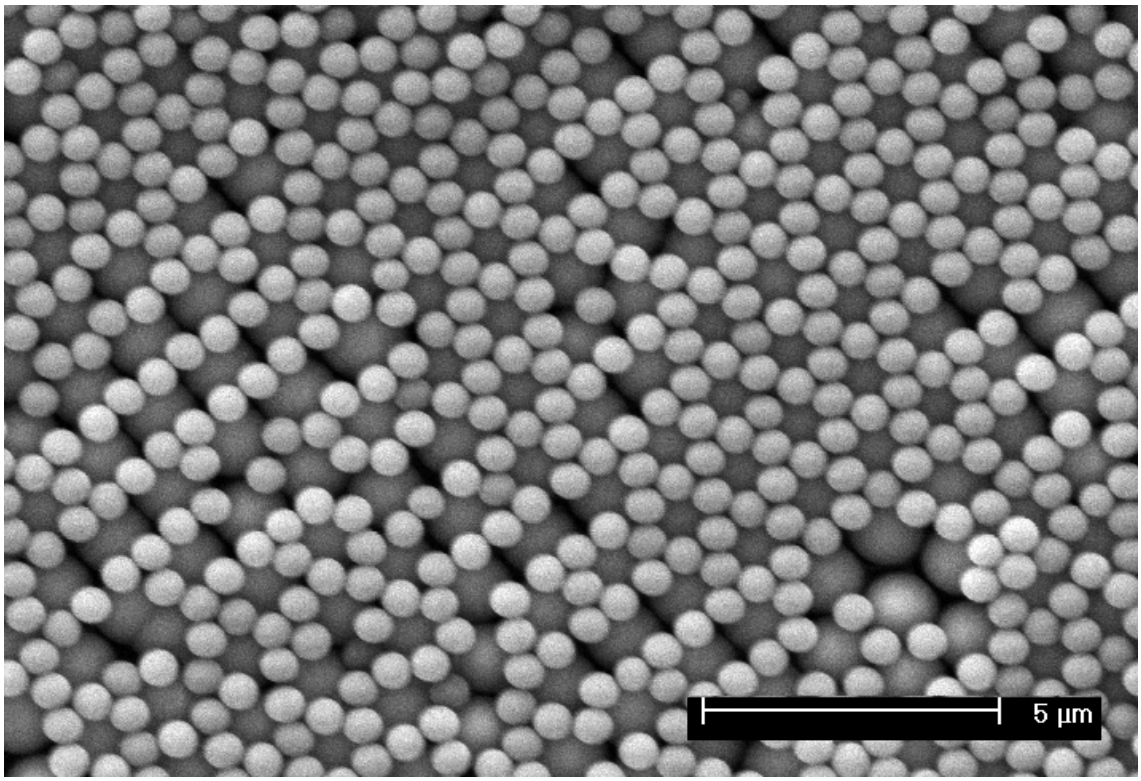

Supplemental Figure 4. Scanning electron micrographs (SEM) showing areas with line-like defects in the *kagomé* (LS_3) net of small spheres on top of a 2D crystal of large spheres (R_L = 716 nm, γ = 0.49).